Geophysical Journal International

Geophys. J. Int. (2013) **195,** 2005–2015
Advance Access publication 2013 October 1

doi: 10.1093/gji/ggt368

A low attenuation layer in the Earth's uppermost inner core

Lauren Waszek and Arwen Deuss

University of Cambridge, Bullard Laboratories Madingley Rise, Cambridge CB3 0EZ, UK. E-mail: lw313@cam.ac.uk

Accepted 2013 September 10. Received 2013 July 18; in original form 2013 March 27

SUMMARY

The attenuation structure of the Earth's inner core, in combination with the velocity structure, provides much insight into its rheological and mineralogical properties. Here, we use a large data set of PKIKP/PKiKP amplitude ratios to derive attenuation models for the upper 100 km of the inner core, incorporating the effects of velocity models calculated using the same data set. We confirm that the upper inner core is hemispherical in attenuation, with stronger attenuation in the east hemisphere. We also observe, for the first time, a low attenuation upper layer of approximately 30 km thickness throughout the top of the inner core. Attenuation increases beneath this layer, and then gradually decreases going deeper into the inner core. Although the data appear to show attenuation anisotropy below 57.5 km depth in the west, we find that this can be explained by the velocity models alone, with no requirement for attenuation anisotropy in the upper inner core.

Key words: Core, outer core and inner core; Body waves; Seismic anisotropy; Seismic attenuation.

1 INTRODUCTION

Over the last few years, seismic studies have greatly furthered our knowledge of the velocity structure in the Earth's inner core. However, large levels of scatter in inner core attenuation data mean that the attenuation properties are much less understood. Velocity anisotropy in the inner core is oriented with the faster polar axis aligned to the Earth's rotation axis (Poupinet *et al.* 1983; Morelli *et al.* 1986; Woodhouse *et al.* 1986). Attenuation investigations suggest that this direction also displays stronger attenuation, resulting in smaller amplitudes (Souriau & Romanowicz 1996; Yu & Wen 2006b; Kazama *et al.* 2008; Souriau 2009). Attenuation anisotropy may also produce broader polar waveforms (Souriau & Roudil 1995), though pulse broadening can also be caused by triplications from velocity discontinuities inside the inner core (Song & Helmberger 1998). Although attenuation anisotropy has been observed to at least 500 km depth (Souriau & Roudil 1995; Yu & Wen 2006b; Souriau 2009; Mäkinen & Deuss 2013), its presence in the upper layers has not been determined (Wen & Niu 2002; Cao & Romanowicz 2004).

Large-scale hemispherical differences also exist in the inner core, with the west hemisphere having a lower velocity, lower attenuation and being more anisotropic than the east hemisphere (Tanaka & Hamaguchi 1997; Creager 1999; Tseng & Huang 2001; Wen & Niu 2002; Cao & Romanowicz 2004; Oreshin & Vinnik 2004; Deuss *et al.* 2010). Attenuation and velocity variations seem correlated, that is, either high velocity and strong attenuation, or low velocity and weak attenuation appear in the same regions (Souriau & Romanowicz 1996; Yu & Wen 2006a,b, 2007; Cormier 2007). However, the depth extent of the correlation is unclear. A hemispherical velocity difference is detected down to 800 km below the inner core boundary (ICB; Oreshin & Vinnik 2004; Irving & Deuss 2011), but the variation in isotropic attenuation disappears at ∼80 km depth (Wen & Niu 2002; Cao & Romanowicz 2004). The upper 100 km of the inner core shows complicated layering in the isotropic and anisotropic velocity structure (Waszek & Deuss 2011); similar constraints on the attenuation structure will help us understand the solidification mechanisms of the inner core.

Another issue arises from the relationship between velocity and attenuation, with regions of high velocity being more strongly attenuating (Souriau & Romanowicz 1996; Wen & Niu 2002; Yu & Wen 2006a,b). This relationship is difficult to explain, especially as the mantle displays the opposite correlation: higher velocity regions display lower attenuation (e.g. Romanowicz & Durek 2000), resulting from temperature differences and the material being cold. Fluid inclusions or partial melting would also be able to produce the mantle observations. In the inner core, the only explanation for the correlation of high velocity with strong attenuation would be the alignment of anisotropic crystals, causing anisotropic scattering and therefore anisotropic energy loss (Bergman *et al.* 2000).

A problem with measuring attenuation is that some of the observed correlation between strong attenuation and high velocity may be an artefact from the hemispherical velocity differences. The velocity jump across the ICB will affect the transmission and reflection coefficients of PKIKP and PKiKP, the seismic phases which are used to study inner core attenuation. Thus, we must also consider attenuation in combination with velocity structure. Although several studies have considered both properties simultaneously (Wen & Niu 2002; Yu & Wen 2006a,b, 2007), their data sets were comparatively small, and suffered a lack of global polar data. Using our larger PKIKP/PKiKP data set, we generate layered attenuation models of the upper 100 km of the inner core, taking into account

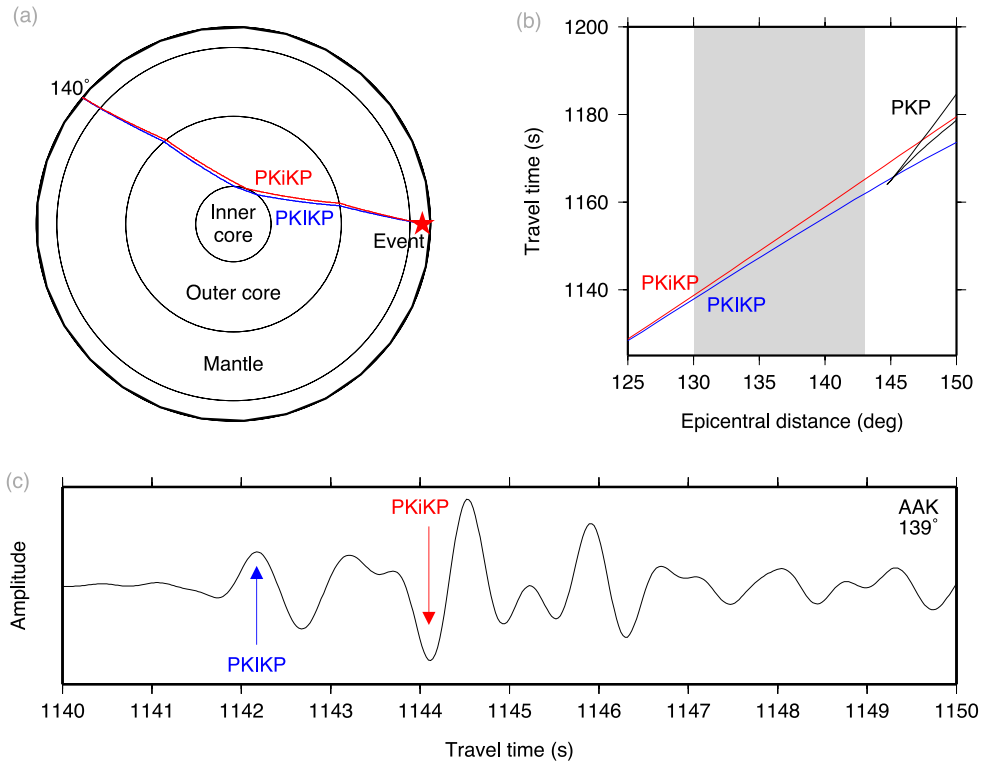

Figure 1. (a) Ray paths of PKIKP (blue) and PKiKP (red) for an event at 100 km depth. (b) Traveltime curves for PKIKP, PKiKP and PKP. The PKIKP and PKiKP phases will be separate, and avoid PKP, for an epicentral distance range of 130°–143°. (c) Seismogram from an event on 2009 September 5 in Peru, narrow bandpass filtered between 0.7 and 2 Hz, observed at an epicentral distance of 139°. The first arrival is the PKIKP phase, which has travelled through the inner core; the outer core reflected phase PKiKP arrives just under 2 s later.

the velocity structure. We are particularly interested in constraining the depth extent of the hemispherical differences, the presence or lack of attenuation anisotropy and any correlation to the velocity structure.

2 DATA AND METHODS

2.1 Data

We study the inner core using the seismic phase PKIKP, which travels through the mantle, outer core and the inner core, and the reference phase PKiKP, which follows the same path as PKIKP but reflects from the ICB (Fig. 1a). The paths diverge only at the top of the inner core, thus differences in their amplitudes result primarily from inner core attenuation of PKIKP, and reflection and transmission coefficients at the ICB. PKIKP and PKiKP are observed as separate phases at event–receiver epicentral distances of 130°–143° (Fig. 1b). At this range, PKIKP has turning depths from 15 to 106 km depth into the inner core.

We require events which are large enough to produce observable phases (magnitudes of $5.2 < M_w < 6.3$) and deep enough to prevent surface reflection interference (depth > 15 km). We filter the data from 0.7 to 2 Hz, to centre on the phases at 1 Hz. We used data from 766 events from 1990 January to 2012 September, and obtained 3102 measurements of PKIKP and PKiKP amplitudes. The large quantity of data now available allow us to select only the highest quality seismograms with low noise levels and well-separated phases, keeping less than 6 per cent of the original data. We pick the phases using cross-correlation, and also check each seismogram manually (Fig. 1c).

2.2 Velocity modelling

Body waves lose energy by intrinsic attenuation, in addition to scattering from heterogeneities, geometrical spreading of the wave front and energy loss at interfaces. Although the ray paths of PKIKP and PKiKP through the mantle are very close, differences arise at the ICB. Using WKBJ (Chapman 1976), we generate synthetic seismograms for PKIKP and PKiKP, and obtain predicted PKIKP/PKiKP amplitude ratios as a function of epicentral distance, incorporating geometrical spreading and energy loss at interfaces. The synthetics are processed in the same way as the observed data. Comparing the predicted amplitude ratios with the observed ones, we attribute the difference to attenuation, and determine Q_α, which is the quality factor corresponding to seismic attenuation.

We investigate the effects of different velocity models on PKIKP/PKiKP amplitude ratios, by calculating predictions for the 1-D earth model AK135 (Kennett *et al.* 1995) and for our own hemispherical and anisotropic velocity models (Waszek & Deuss 2011). Our velocity models are updated to include new data (Fig. 2), and referred to as WD11 from here. The models are perturbations to AK135 in the upper 110 km of the inner core (extended to 150 km to include all possible PKIKP turning depths), and separated into three depth layers: 15–30 km (upper layer), 30–57.5 km (middle) and 57.5–106 km (lower). These layers correspond to physical structures in the inner core. The east hemisphere has a high velocity upper layer of 30 km thickness. The west hemisphere has a sharp discontinuity at 57.5 km depth, which separates an isotropic upper layer from 2.8 per cent anisotropy in the deeper inner core. Only this interface in the western polar model is sharp enough to produce reflections, so we smooth out all other discontinuities. As we do not have PKIKP paths, which turn in the upper 15 km of the inner core,

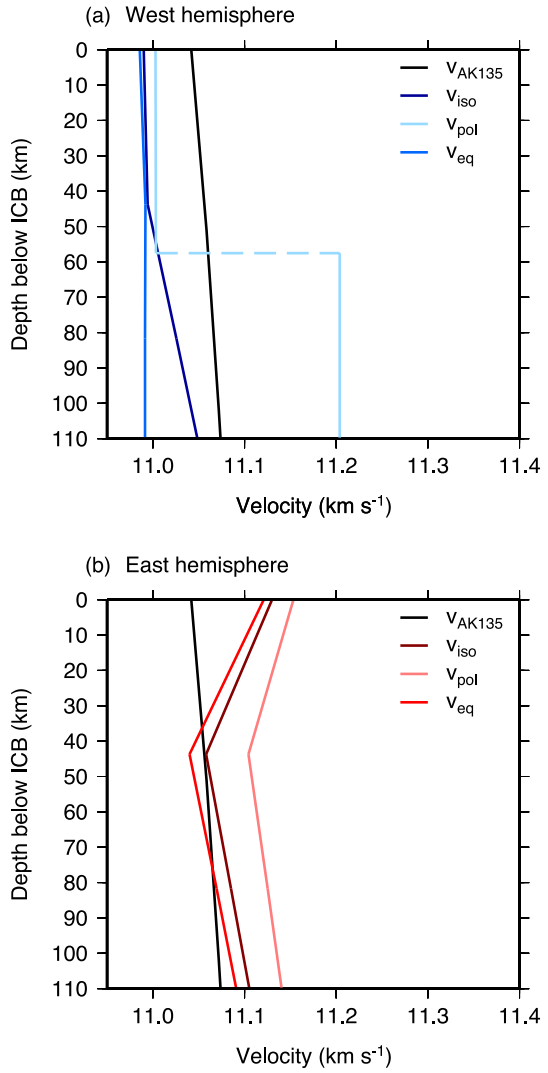

Figure 2. Velocity models for the upper inner core based on those calculated by Waszek & Deuss (2011). The model has been extended to the ICB and to 150 km below the ICB; outside of these ranges, AK135 is used. Discontinuities in velocity that do not correspond to sharp interfaces have been smoothed.

the upper layer is actually an average of the top 30 km. We therefore extend the upper layer to the ICB to produce a hemispherical difference in velocity jump, which has been detected in previous studies (Wen & Niu 2002; Yu & Wen 2006a).

2.3 Attenuation modelling

The observed and synthetic PKIKP/PKiKP amplitude ratios are used to determine the attenuation structure along the PKIKP ray path as follows (Aki & Richards 1980):

$$\frac{(A_{\mathrm{PKIKP}}/A_{\mathrm{PKiKP}})_{\mathrm{obs}}}{(A_{\mathrm{PKIKP}}/A_{\mathrm{PKiKP}})_{\mathrm{syn}}} = \mathrm{e}^{-\pi\omega t^*} \quad (1)$$

and

$$t^* = t/Q_\alpha, \quad (2)$$

where A is amplitude, ω is the wave frequency (1.0 Hz), t is the traveltime of PKIKP in the inner core and Q_α is the quality factor of the seismic attenuation. The synthetics which are calculated using WKBJ incorporate losses from spreading and interfaces, but not intrinsic attenuation. We simulate inner core attenuation by applying a t^* filter to the synthetic PKIKP signal; the t^* value is calculated using eq. (2). A forward modelling approach is used to determine the best-fitting attenuation structure, by selecting the Q_α value which minimizes the L2 misfit between the synthetic and the average observed PKIKP/PKiKP amplitude ratios. The errors in Q_α correspond to the value that fits within one standard deviation of the observations.

2.4 Anisotropy

Anisotropy in attenuation refers to a dependence of Q_α on direction. It is defined by the angle between the PKIKP ray path at its turning point and the Earth's rotation axis, ζ. For polar paths $\zeta < 35^\circ$, and for equatorial paths $\zeta > 35^\circ$. Inner core anisotropy is oriented about the Earth's rotation axis, and produces smaller amplitudes for waves travelling in polar directions (Souriau & Romanowicz 1996; Yu & Wen 2006b). We investigate directional variations in amplitude ratios using the following equations for weak anisotropy (modified from Creager 1992):

$$A_{\mathrm{PKIKP}}/A_{\mathrm{PKiKP}} = a + b\cos^2\zeta + c\cos^4\zeta, \quad (3)$$

where a, b and c are related to the Love coefficients (Love 1927). The equatorial direction corresponds to $\zeta = 90^\circ$ and the polar direction to $\zeta = 0^\circ$, therefore:

$$(A_{\mathrm{PKIKP}}/A_{\mathrm{PKiKP}})_{\mathrm{eq}} = a, \quad (4)$$

$$(A_{\mathrm{PKIKP}}/A_{\mathrm{PKiKP}})_{\mathrm{pol}} = a + b + c. \quad (5)$$

The strength of anisotropy is subsequently calculated by taking the difference between the polar and equatorial ray paths:

$$\Delta A_{\mathrm{ani}} = (A_{\mathrm{PKIKP}}/A_{\mathrm{PKiKP}})_{\mathrm{pol}} - (A_{\mathrm{PKIKP}}/A_{\mathrm{PKiKP}})_{\mathrm{eq}} = b + c. \quad (6)$$

3 RESULTS

3.1 Observed PKIKP/PKiKP amplitude ratios

We first examine the PKIKP/PKiKP amplitude ratio data for any obvious regional or anisotropic structures (Fig. 3). Due to high levels of scatter in the amplitude ratio data, we cannot use it to determine hemisphere boundaries by visual inspection, and use the hemisphere boundaries of Waszek *et al.* (2011). We partition the data further into epicentral distance ranges which correspond approximately to the upper, middle and lower depth layers defined in the velocity models (Fig. 2). Examining all the data, the western hemisphere (Fig. 4a) has larger average amplitude ratios than the eastern hemisphere (Fig. 4b), meaning PKIKP is larger compared to PKiKP in the west hemisphere than in the east. Without further analysis, this would correspond to a more attenuating east hemisphere, as has been observed in many previous studies (Tseng & Huang 2001; Wen & Niu 2002; Oreshin & Vinnik 2004; Yu & Wen 2006a). Our amplitude ratios also show a general increase with epicentral distance.

As the hemispherical differences are small, we perform statistical tests to determine whether they are significant (results in Table S1). The difference in mean amplitude ratio is studied using a *t*-test, and the difference in variance using an *f*-test. The hemispherical difference in mean amplitude ratio is significant at the 1 per cent level at all depths. This tells us that the probability that there is no difference between the hemispheres is less than 1 per cent. Comparing

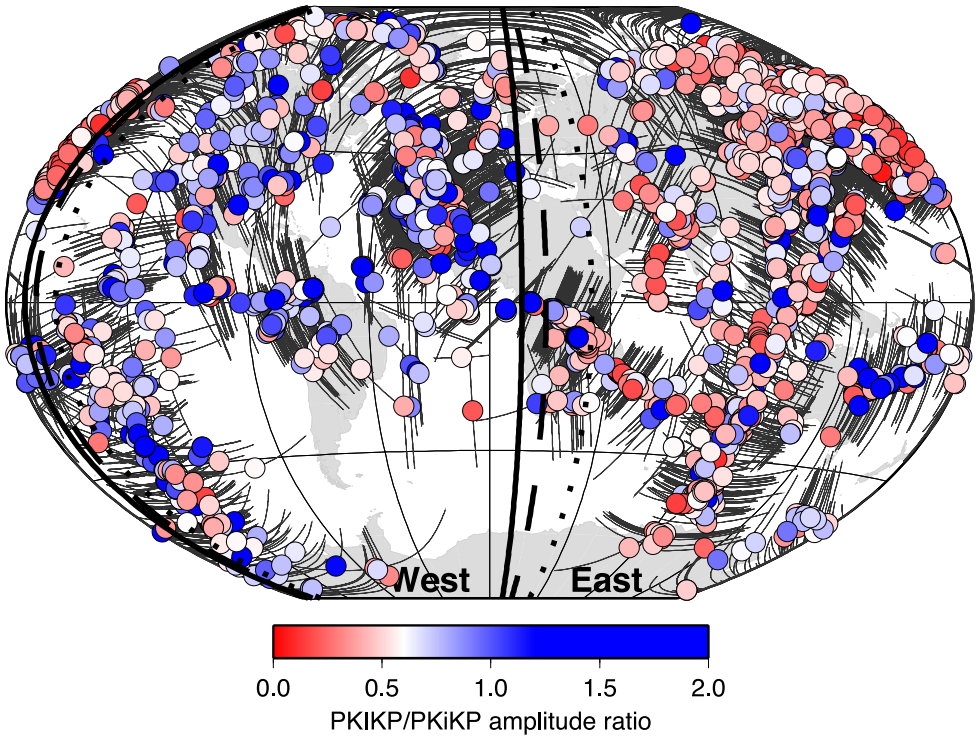

Figure 3. Map showing the observed PKIKP/PKiKP amplitude ratios. Thin lines indicate PKIKP ray paths through the inner core, and the locations of the circles correspond to the turning points of the PKIKP rays. Colours of the circles indicate the PKIKP/PKiKP amplitude ratios. Hemisphere boundaries as a function of PKIKP turning depth are shown for each depth layer below the ICB as the thick black lines: solid line 15–30 km, dashed line 30–57.5 km and dotted line 57.5–106 km.

the variance, we find that the stronger scattering in the middle and lower layers in the west hemisphere is significant at the 1 per cent level. In the upper layer, the east hemisphere is more scattered, which is significant at the 5 per cent level. The amount of scatter may indicate how much of the energy loss is a result of scattering from heterogeneities (Cormier *et al.* 1998). For example, smaller grains in the east may create greater scatter (Cormier 2007; Leyton & Koper 2007). Scatter in the observed amplitude ratios is also produced by random noise in the seismograms. Most of our data have a signal-to-noise ratio of 5–10 (Fig. S1), which corresponds to a spread of 10–20 per cent in the amplitude ratios, and may explain some of the scatter in our data.

Attenuation anisotropy in the deeper inner core has previously been observed in PKIKP/PKPbc data, with smaller PKIKP amplitudes in the polar direction (Souriau & Romanowicz 1996; Yu & Wen 2006b; Kazama *et al.* 2008; Souriau 2009). We investigate if a difference between the polar and equatorial PKIKP/PKiKP amplitude ratios is visible in our data, as it would indicate anisotropy in attenuation also exists at the top of the inner core. We find that only the lower layer of the west hemisphere displays smaller amplitude ratios in the polar than equatorial direction (Figs 4c and e). However, we have so far ignored the effects of velocity structure, thus further analysis is required to determine if this attenuation anisotropy is significant.

3.2 Modelling the effects of velocity and t^* on PKIKP/PKiKP amplitude ratios

3.2.1 Velocity models

The specific details of the inner core velocity model used in our synthetic calculations affect the arrival time, amplitude and waveform of PKIKP and PKiKP. For example, a larger velocity jump across the ICB will decrease the transmission coefficient and increase the reflection coefficient, producing a smaller PKIKP/PKiKP amplitude ratio. So, smaller PKIKP/PKiKP ratios could either be due to stronger inner core attenuation, or a larger velocity jump at the ICB, or a combination of both. In addition, we must model structures such as discontinuities and velocity gradients inside the inner core.

Fig. 5 contains synthetic PKIKP and PKiKP signals generated for reference model AK135 and our WD11 velocity models for the west and east hemisphere, at distances of 130°, 136.5° and 143°. Although no attenuation is included, the PKIKP amplitudes vary notably between the models. For the isotropic WD11 model, the PKIKP/PKiKP amplitude ratios are smaller in the east hemisphere (Fig. 5c) and larger in the west (Fig. 5b), an effect which is solely a result of the different velocity jumps across the ICB without the need for hemispherical variation in Q_α.

Examining the polar direction in the western hemisphere (Fig. 5f), we find that the seismograms at 130° and 136.5° are complicated by triplication arrivals. The PKIKP/PKiKP amplitude ratios in the polar direction (Fig. 5f) is larger than in the equatorial direction (Fig. 5d) at 136.5°, but smaller at 143°. We find similar variations in synthetic amplitude ratios for the eastern hemisphere (Fig. 5g). These differences will affect our anisotropy modelling, so it is essential that we incorporate velocity structure.

3.2.2 The t^* filter

We synthesize inner core attenuation by applying a t^* filter to the synthetic PKIKP waveforms. The observed PKIKP/PKiKP amplitude ratios are shown in Fig. 6, with PKIKP/PKiKP amplitude predictions for Q_α values of 200, 300 and 400, and with no attenuation

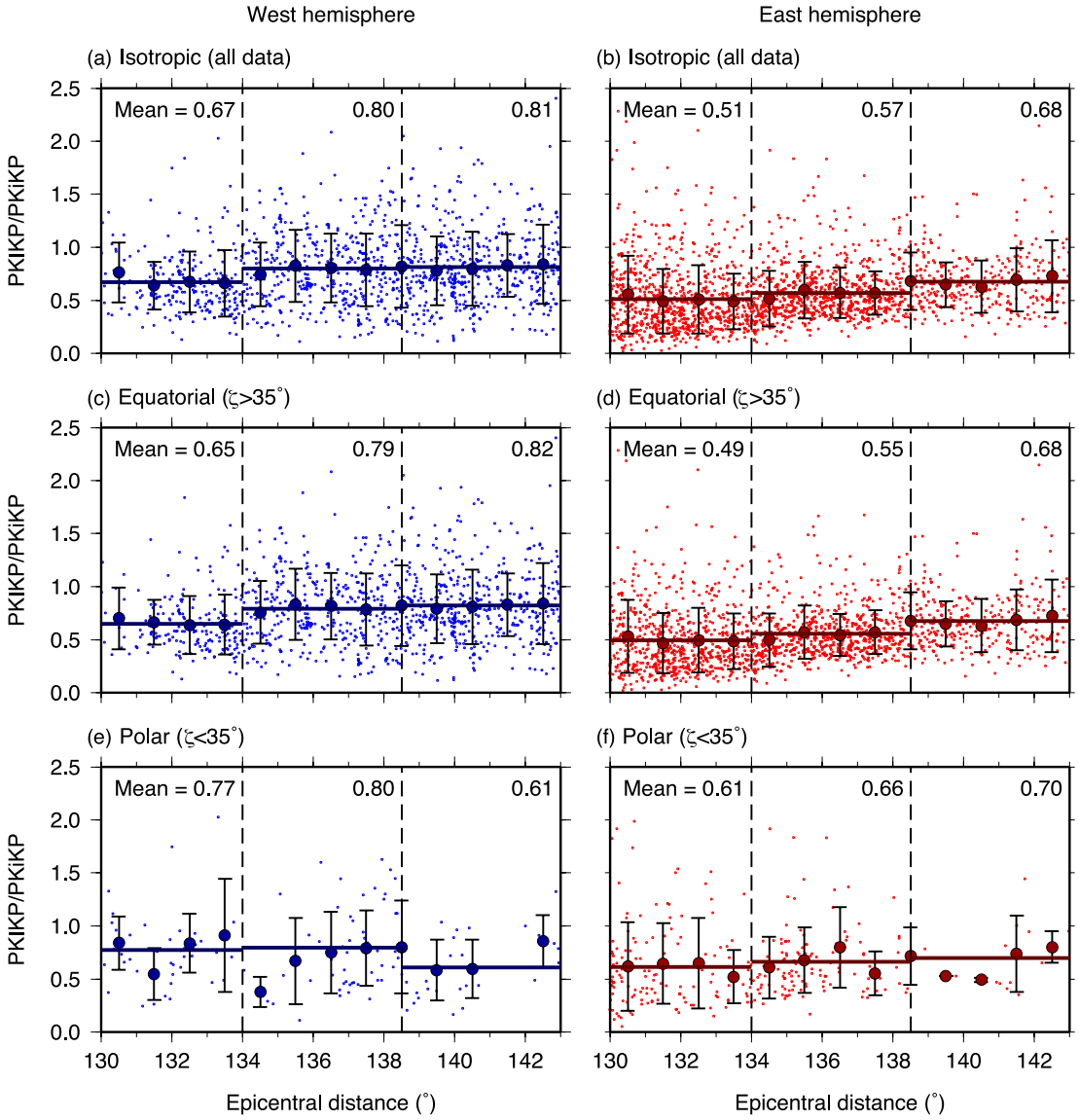

Figure 4. PKIKP/PKiKP amplitude ratios as a function of epicentral distance, separated according to hemisphere. Plots show all of the data, equatorial data ($\zeta > 35°$) and polar data ($\zeta < 35°$). The large circles correspond to average PKIKP/PKiKP amplitude ratio values taken for 1° bins. Vertical error bars indicate the standard deviation on the average amplitude ratio, which indicates scatter. Horizontal lines correspond to the average amplitude ratios in the epicentral distances of 130°–134°, 134°–138.5° and 138.5°–143°.

(i.e. $Q_\alpha \rightarrow \infty$). L2 misfits are contained in Table 1. Without attenuation, the predicted ratios are too large, confirming the need for inner core attenuation. In Fig. 6 we also see the effects of different velocity models on amplitude ratios. For example, the east hemisphere models have smaller amplitude ratios at short epicentral distances due to the larger velocity jump at the ICB. We also observe the effects of the discontinuity in the western polar model at 57.5 km depth, giving rise to waveform complexities and increased amplitudes at distances less than ∼139° (Fig. 6g).

Examining the AK135 predictions (Figs 6a and b), we find that Q_α of 300–400 is closest to the observed amplitude ratios in the west hemisphere, whereas 200–300 best explains the east hemisphere. This indicates a hemispherical difference in attenuation when using just AK135, in agreement with previous studies. Comparing the WD11 isotropic and equatorial predictions with observed data in the west hemisphere (Figs 6c and e), only Q_α of 300 falls within one standard deviation of the average amplitude ratios. In the east hemisphere, the isotropic and equatorial data (Figs 6d and f) are best fit with Q_α of 200. Thus, a difference between the two hemispheres, with east being more attenuating than west, is also seen using the WD11 models. The polar amplitude ratios have large fluctuations due to lack of data, and no single Q_α model can explain the polar data (Figs 6g and h). Looking in more detail, the predicted ratios are all too large at greater epicentral distances, and too small at short distances. This requires a layered Q_α structure, with a higher Q_α in the upper layer of both hemispheres.

3.3 Isotropic attenuation structure

We next determine layered Q_α models through minimizing the L2 misfits (Table 1), generating an average model incorporating AK135, and also hemispherical models using either AK135 or WD11 (Fig. 7). Errors correspond to the Q_α which fits the data within one standard deviation. We find that the Q_α models obtained

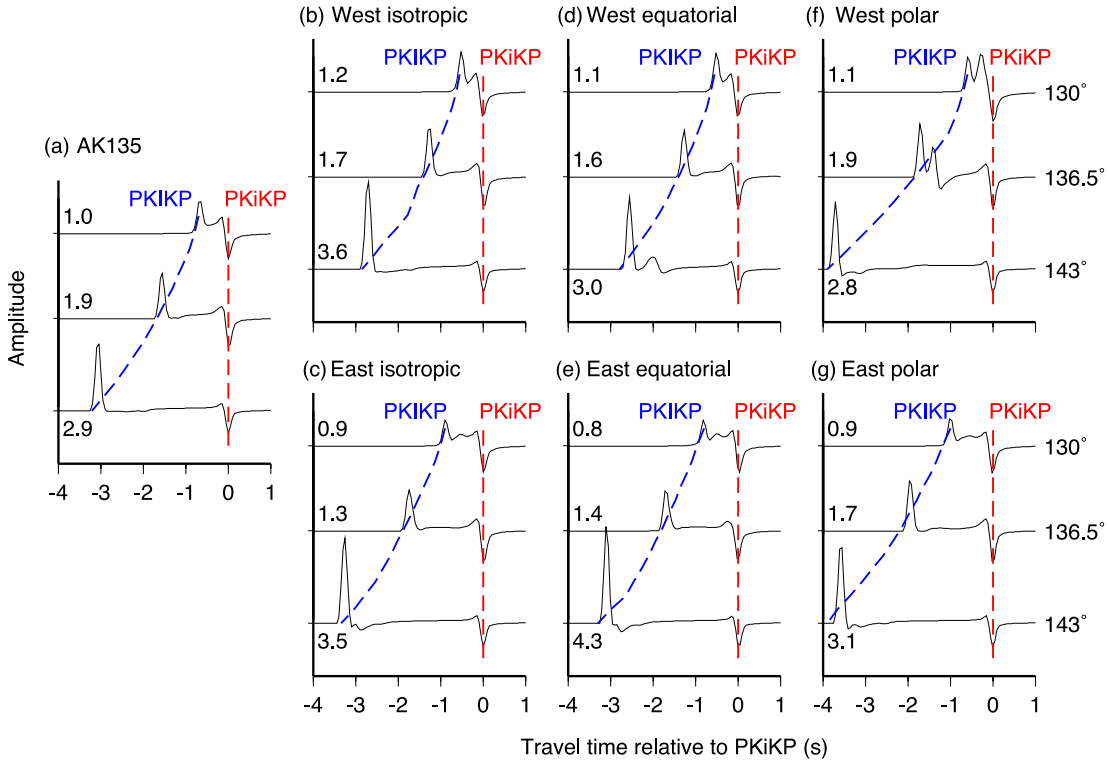

Figure 5. Synthetic traces of PKIKP and PKiKP at epicentral distances of 130°, 136.5° and 143° generated for the different velocity models of (a) AK135, and the isotropic and anisotropic west (b, d, f) and east (c, e, g) hemisphere models from Fig. 2. The traces are aligned on the PKiKP arrival (red lines) and the PKIKP predicted arrival times for each model are indicated (blue lines). The PKIKP/PKiKP amplitude ratios are indicated at the left of each trace.

using AK135 are within error bounds of the WD11 Q_α models. Additionally, we have also calculated Q_α models using synthetics with and without real noise, and find that its effect is negligible.

The hemispherical Q_α models (Figs 7b and c) are a superior match to the data than the average model (Fig. 7a). The east hemisphere and average models are very similar, and the misfits are nearly identical. However, the west hemisphere model differs from the average model, and has a much smaller misfit. We use an *f*-test to compare the residual errors between models, which shows that the hemispherical model is a better fit than the average model with a 1 per cent level of significance. This means that the probability of observing this difference in misfits with no hemispherical structure is less than 1 per cent. Thus, our layered models also confirm a hemispherical difference in Q_α. Looking in more detail, we find that the hemispherical difference is confined to the upper 57.5 km of the inner core. Here, the west hemisphere has higher Q_α values than the east hemisphere, with best-fit values of 525 in the upper layer and 200 in the middle layer in the west, compared to 425 and 125 in the east. Thus, the west hemisphere is less attenuating than the east, in agreement with Tseng & Huang (2001), Wen & Niu (2002) and Yu & Wen (2006a). We therefore observe the same correlation between low velocity and weak attenuation, and high velocity and strong attenuation, that has been found in earlier work (Song & Helmberger 1998; Oreshin & Vinnik 2004; Yu & Wen 2006b). Deeper than 57.5 km depth in the inner core, the hemispherical difference disappears and Q_α converges to 225.

Examining depth variation, both hemispheres display the same high Q_α, low attenuation upper layer. As discussed, observational evidence for this layer can be seen in Fig. 6 as higher amplitude ratios at shorter distances. Cao & Romanowicz (2004) reported a high Q_α upper layer in the west hemisphere only, and not in the east. Their model starts at 32 km below the ICB, which is deeper than our upper layer. Therefore, our models are in agreement if the high Q_α layer in the east is limited to the upper 32 km of the inner core. Regional studies by Kazama *et al.* (2008) and Iritani *et al.* (2010) also found a high Q_α upper layer in the inner core, however their depth layers are 100 km thick and so we cannot compare their results to our observations.

3.4 Anisotropic attenuation structure

Anisotropy in attenuation has previously been observed as variation in PKIKP/PKPbc amplitude ratios with the angle ζ between the ray path in the inner core and the Earth's rotation axis (Souriau & Romanowicz 1996). On the other hand, we have shown that some variation in PKIKP/PKiKP amplitude ratios can result from variations in velocity structure only. Attenuation causes greater damping of higher frequencies (Aki & Richards 1980), and thus attenuation anisotropy should produce broader PKIKP waveforms for polar paths. Alternatively, Song & Helmberger (1998) showed that broadening of the waveforms can also arise from interaction with discontinuities, which causes triplications. Therefore, pulse broadening may not be indicative of attenuation anisotropy either. Here, we investigate these effects.

First, we examine attenuation anisotropy by performing a linear inversion of the PKIKP/PKiKP amplitude ratios, fitting eq. (3) to the data to determine the *a*, *b* and *c* coefficients (Table S2). Fig. 8 contains the PKIKP/PKiKP amplitude ratios as a function of ζ, with the lines of best fit. The difference between polar and equatorial amplitude ratios is given by ΔA_{ani}. A negative value indicates a lower Q_α (i.e. stronger attenuation) in the polar direction. Although the data are very scattered, we find that the *b* and *c* coefficients

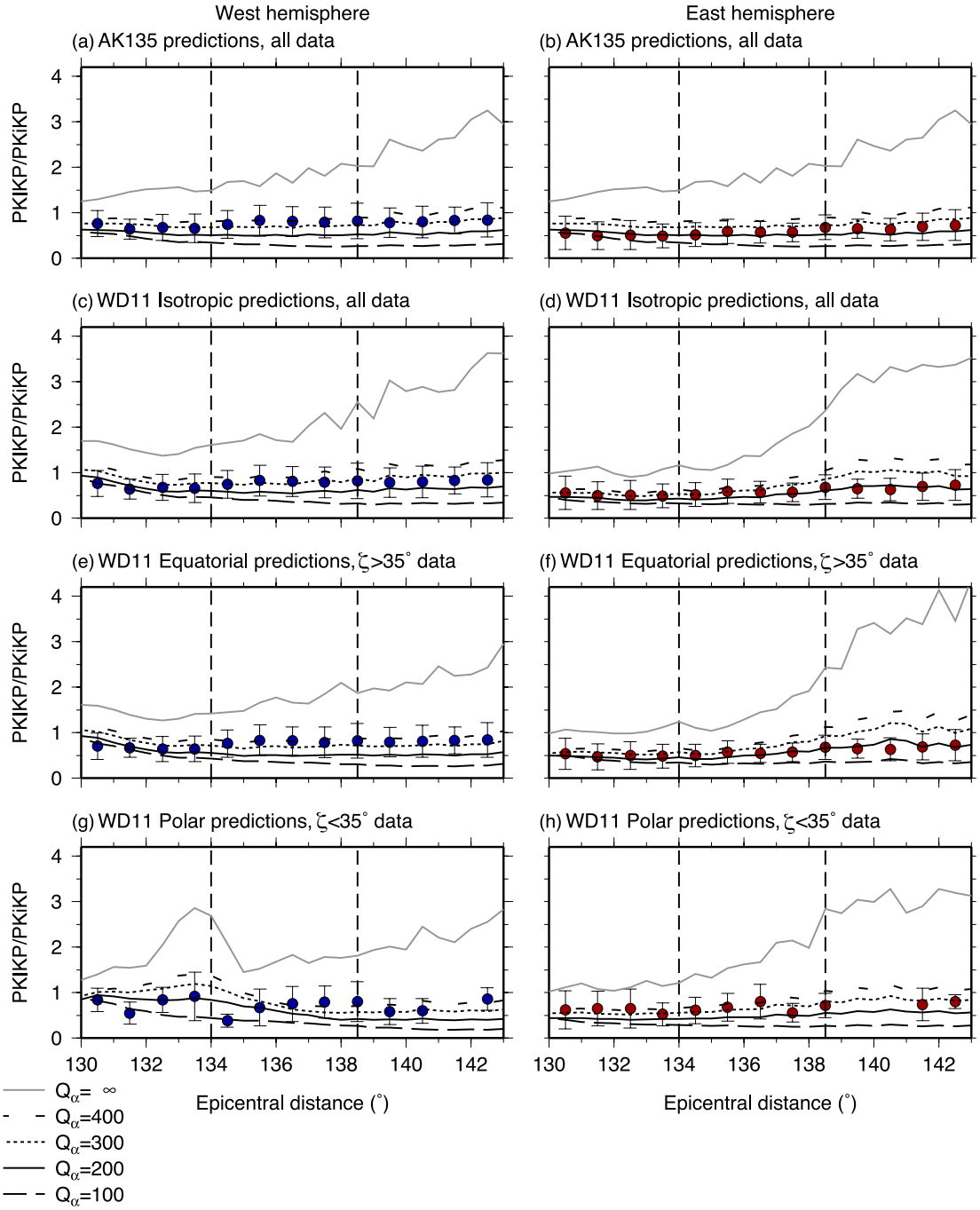

Figure 6. Average observed PKIKP/PKiKP amplitude ratios as a function of event–receiver epicentral distance, separated by hemisphere (red and blue circles). The lines superimposed over the data are the predicted PKIKP/PKiKP amplitude ratios measured from synthetics calculated for the AK135 and WD11 models with different values of Q_α. Both the observed and synthetic data have been filtered in the same way.

are significant at the 1 per cent level in the middle and lower layers of the west hemisphere, and only the lower layer has a significant difference between the polar and equatorial directions (Fig. 8c). In the lower layer, $\Delta A_{\rm ani} = -0.33$, which means that the polar direction is more attenuating, in agreement with previous studies (Souriau & Romanowicz 1996; Yu & Wen 2006b).

Next, we investigate the effects of velocity structure, which may explain some of the apparent observed attenuation anisotropy. We recreate Fig. 8 using synthetic data (Fig. 9), using the WD11 models for a range of ζ values and epicentral distances. No attenuation is included, so Fig. 9 shows the variation in amplitude ratio due to anisotropic velocity structures alone. Comparing the shape of the fitted curves, we find a good correspondence between the predictions and observations. The anisotropic velocity synthetics simulate the effects of attenuation anisotropy, and in particular, the middle and lower layers of the west hemisphere are matched extremely well (Figs 9b and c). For the lower layer, the synthetics predict smaller polar amplitudes than equatorial (Fig. 9c), in strong agreement with the observed data. We therefore find that our velocity models alone can reproduce much of the observed anisotropy in amplitude ratios.

In Fig. 10, we investigate the waveforms of data from the west hemisphere for broadening of the PKIKP pulse compared to PKiKP.

Table 1. L2 misfits of single layer Q_α structures (corresponding to Fig. 6), and for the best-fitting three layered structures (corresponding to Fig. 7).

	Q_α	200	300	400	Three layers
All data	AK135	0.053	0.009	0.056	0.004
					West: 0.020; East: 0.011
West	AK135	0.118	0.029	0.045	0.010
	Isotropic	0.080	0.034	0.101	0.006
	Equatorial	0.127	0.030	0.020	-
	Polar	0.135	0.149	0.243	-
East	AK135	0.028	0.018	0.090	0.004
	Isotropic	0.036	0.087	0.227	0.010
	Equatorial	0.043	0.113	0.272	-
	Polar	0.095	0.043	0.071	-

We compare shallow and deep rays in polar and equatorial directions. In the observed data, only the shallow polar PKIKP signal shows broadening with respect to PKiKP (Fig. 10a). We do not observe broadening of the PKIKP in the deeper polar path (Fig. 10b), or in the equatorial paths (Figs 10c and d). Our observations would be consistent with attenuation anisotropy in the upper 57.5 km of the west hemisphere (Souriau & Romanowicz 1996). However, the broadening could be due to the velocity structure instead. To investigate, for each path we calculate the WD11 velocity models for the corresponding ζ and generate synthetics without attenuation. The sharp velocity discontinuity at 57.5 km depth in the west hemisphere results in a triplication in the shallow polar path; we produce synthetics with and without the extra phases arising from the discontinuity. We note the seismogram with the extra phases from the triplication has a broader PKIKP signal than the seismogram with only PKIKP and PKiKP (Fig. 10a). This means that the PKIKP pulse appears broadened due to the discontinuity at 57.5 km, in agreement with Song & Helmberger (1998). Thus, the PKIKP/PKiKP amplitude ratios and waveform complexities in the west hemisphere are explained by layered anisotropy velocity model instead, and require no attenuation anisotropy.

4 DISCUSSION

The hemispherical differences in velocity and attenuation we observe in the upper inner core have been proposed to arise from two different mechanisms. Thermochemical flow in the outer core may couple the thermal structure at the core–mantle boundary to the inner core, generating a difference in cooling rates at the ICB, by removing more heat from the east hemisphere (Sumita & Olsen 1999; Aubert *et al.* 2008). More rapid and random solidification in the east then produces an isotropic structure with higher velocity and stronger attenuation, and with greater scattering due to smaller grains (Cormier 2007). Slower cooling in the west allows anisotropy to develop. Alternatively, the inner core may translate laterally eastwards, driven by melting in the east hemisphere and freezing in the west (Alboussière *et al.* 2010; Monnereau *et al.* 2010). Annealing during translation results in the hemispherical difference in textures observed seismically (Bergman *et al.* 2010). It is difficult to distinguish between the two mechanisms, but we prefer the thermochemical flow model by Aubert *et al.* (2008) because it suggests that the east hemisphere contains smaller grain sizes, explaining the higher scatter seen in our data.

We also find a low attenuation layer at the top of the inner core, which may be linked to growth processes of the ICB. There are two proposed solidification mechanisms of the inner core. The growth may be dendritic (Fearn *et al.* 1981), with solidification occurring in a mushy boundary layer (Roberts *et al.* 2003). Conversely, the inner core may grow through precipitation (Shimuzu *et al.* 2005; Zou *et al.* 2008), accompanied by a slurry layer at the ICB. Fluid inclusions in these layers increase attenuation (Singh *et al.* 2000). As the inner core solidifies, fluid is expelled (Loper 1983) and attenuation decreases with depth. This is what we observe beneath 30 km depth. However, these processes cannot explain the low attenuation upper layer. Cao & Romanowicz (2004) proposed that the low attenuation layer in the west hemisphere represents the top of an extended solidification zone. A high melt fraction in the layer results in interconnection of the fluid to produce low attenuation (Bergman 2003). Attenuation increases at the point where the fluid becomes separate inclusions; in our model, this corresponds to 30 km depth. However, we previously determined that there is no sharp discontinuity at this depth in either hemisphere (Waszek & Deuss 2011). Furthermore, a sharp ICB with a thin mushy layer (much less than 30 km) is required to explain observations of PKiKP (Cummins & Johnson 1988), and PKJKP (Deuss *et al.* 2000). The existence of a layer with interconnected fluid at the top of the inner core therefore seems unlikely, leaving the reason for a low attenuation upper layer unclear.

Finally, we showed that observations of the directional variation in PKIKP/PKiKP amplitude ratios and the PKIKP pulse broadening can be explained by the layered anisotropic velocity structure only. Thus, we do not require attenuation anisotropy in the upper 100 km of the inner core. Our results are not incompatible with

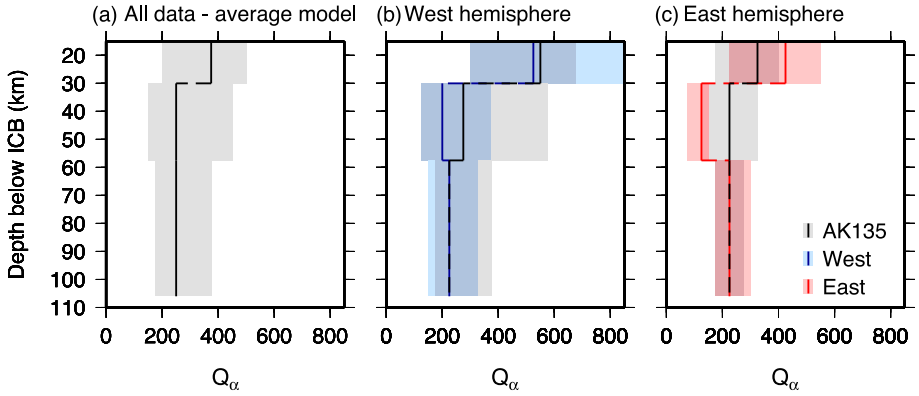

Figure 7. Isotropic Q_α models determined for (a) all data, the average model, and (b) for the west (blue) and (c) east (red) hemispheres. The blue and red lines correspond to models which incorporate our hemispherical and anisotropic velocity models, WD11. Grey lines show the results for AK135. Layers are derived from the technique and do not correspond to sharp boundaries except where indicated in the velocity structure.

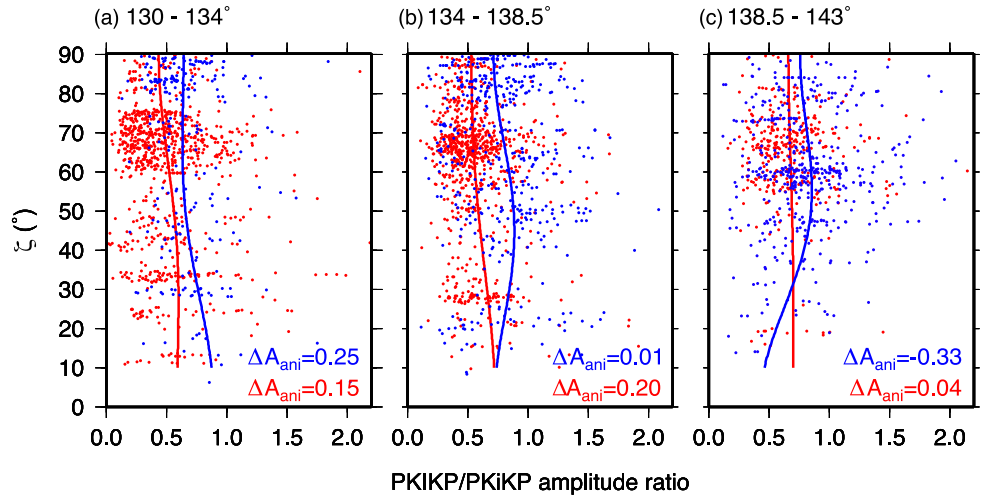

Figure 8. PKIKP/PKiKP amplitude ratios as a function of ζ. West hemisphere data are blue, east are red. The blue and red lines correspond to the fit of eq. (3) to the respective data sets. ΔA_{ani} corresponds to the difference in amplitude ratios between the equatorial and polar direction (eq. 6).

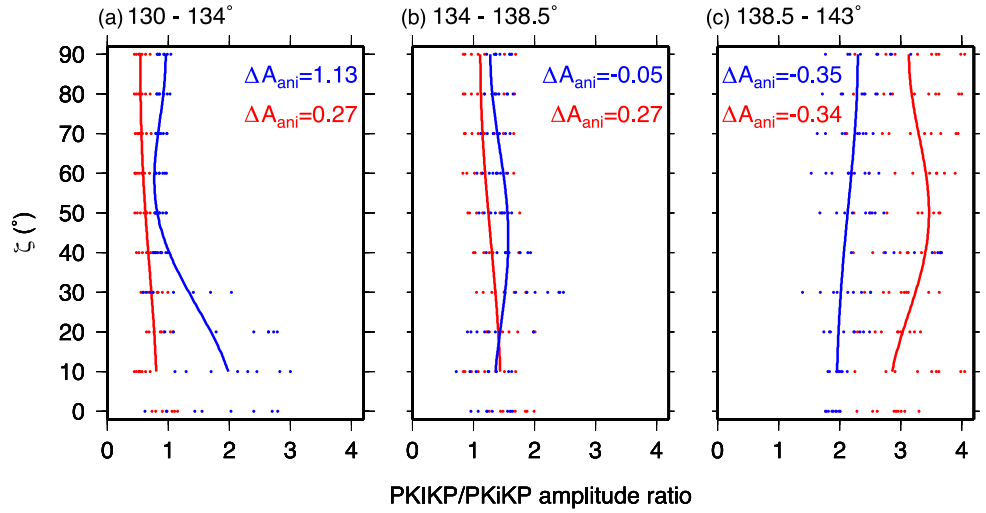

Figure 9. Predicted PKIKP/PKiKP amplitude ratios as a function of ζ, partitioned according to hemisphere and epicentral distance as in Fig. 8. Blue points are predicted amplitude ratios for the west hemisphere and red for the east hemisphere, and the lines correspond to the fit of eq. (3) to the respective data sets. The anisotropic strength, which corresponds to the difference in amplitude ratios between the equatorial and polar direction, is included.

the attenuation anisotropy in the deeper inner core that has been observed before (Souriau & Romanowicz 1996; Yu & Wen 2006b; Kazama *et al.* 2008; Mäkinen & Deuss 2013). It may be possible that the upper inner core is weakly anisotropic in attenuation, but we cannot extract the signal from our data due to the large scatter and dominant effects of the velocity structure. Alternatively, as the velocity is mostly isotropic in the uppermost inner core (Shearer 1994; Ouzounis & Creager 2001; Waszek & Deuss 2011), the relationship between attenuation and velocity would suggest the attenuation structure to be isotropic too (Souriau & Romanowicz 1996; Wen & Niu 2002; Yu & Wen 2006a,b).

5 CONCLUSIONS

We have derived attenuation models for the upper 100 km of the inner core, incorporating hemispherical and anisotropic velocity structure. Our observations confirm a small but significant east–west hemispherical difference in the attenuation structure of the upper inner core, with the east more strongly attenuating than the west. The difference is largest in the upper 30 km, and becomes negligible below 57.5 km depth. This may result from a difference in solidification processes, such as different cooling rates at the ICB (Aubert *et al.* 2008) or translation of the inner core (Alboussière *et al.* 2010; Monnereau *et al.* 2010). Both hemispheres are characterised by the presence of a low attenuation upper layer of approximately 30 km thickness. Such a global layer has not previously been detected, and the underlying cause is currently unexplained. A large increase in attenuation below 30 km depth is then followed by a steady decrease going deeper into the inner core. We find no evidence for attenuation anisotropy in the upper inner core, in agreement with an isotropic velocity structure. Any directional variation in our data can be explained using the hemispherical and anisotropic variation in velocity structure alone, without the need for attenuation anisotropy.

ACKNOWLEDGEMENTS

The research was funded by the European Research Council under the European Community's Seventh Framework Programme

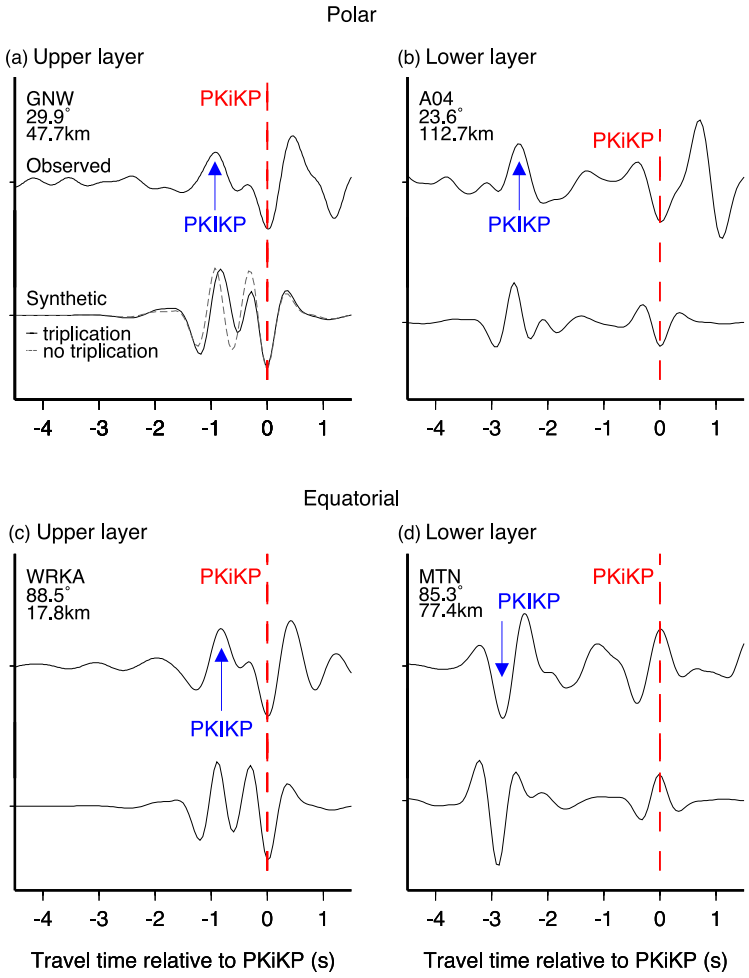

Figure 10. Observed and synthetic seismograms for PKIKP and PKiKP ray paths in the west hemisphere. Polar paths (a, b) are from an event in the South Sandwich Islands on 2004 September 11, and equatorial paths (c, d) are from an event in Argentina on 2012 June 2. The station, PKIKP angle ζ and PKIKP turning depth below the ICB are included with each panel. A velocity model specific to the source function and direction was produced for each ray path, and used to generate the synthetics, using parameters from the WD11 velocity model. The synthetics have been filtered, but have no attenuation, corresponding to infinite Q_α.

(FP7/2007-2013)/ERC grant 204995. AD is also funded by a Leverhulme Prize. LW is funded by a research fellowship from Homerton College, University of Cambridge. We thank two anonymous reviewers for helpful and constructive comments.

REFERENCES

Aki, K. & Richards, P., 1980. *Quantitative Seismology*, Freeman and Co..

Alboussière, T., Deguen, R. & Melzani, M., 2010. Melting-induced stratification above the Earth's inner core due to convective translation, *Nature,* **466,** 744–747.

Aubert, J., Amit, H., Hulot, G. & Olson, P., 2008. Thermochemical flows couple the Earth's inner core growth to mantle heterogeneity, *Nature,* **454,** 758–762.

Bergman, M., 2003. Solidification of the Earth's core, in *Earth's Core: Dynamics, Structure, Rotation, Geodyn. Ser.,* Vol. 31, pp. 105–127, eds Dehant, V., Creager, K., Karato, S. & Zatman, S., AGU

Bergman, M., Giersch, L., Hinczewski, M. & Izzo, V., 2000. Elastic and attenuation anisotropy in directionally solidified (hcp) zinc, and the seismic anisotropy in the Earth's inner core, *Phys. Earth. planet. Inter.,* **117,** 139–151.

Bergman, M., Lewis, D., Myint, I., Slivka, L., Karato, S. & Abreu, A., 2010. Grain growth and loss of texture during annealing of alloys, and the translation of Earths inner core, *Geophys. Res. Lett.,* **37,** L22313, doi:10.1029/2010GL045103.

Cao, A. & Romanowicz, B., 2004. Hemispherical transition of seismic attenuation at the top of the Earth's inner core, *Earth. planet. Sci. Lett.,* **228**(3–4), 243–253.

Chapman, C., 1976. A first motion alternative to geometrical ray theory, *Geophys. Res. Lett.,* **3,** 153–156.

Cormier, V., 2007. Texture of the uppermost inner core from forward- and back-scattered seismic waves, *Earth. planet. Sci. Lett.,* **258,** 442–453.

Cormier, V., Xu, L. & Choy, G., 1998. Seismic attenuation of the inner core: viscoelastic or stratigraphic? *Geophys. Res. Lett.,* **25,** 4019–4022.

Creager, K., 1992. Anisotropy of the inner core from differential travel times of the phases PKP and PKIKP, *Nature,* **356,** 309–314.

Creager, K., 1999. Large-scale variations in inner core anisotropy, *J. geophys. Res.,* **104,** 23 127–23 139.

Cummins, P. & Johnson, L., 1988. Short-period body wave constraints on properties of the Earth's inner core boundary, *J. geophys. Res.,* **93,** 9058–9074.

Deuss, A., Woodhouse, J., Paulssen, H. & Trampert, J., 2000. The observation of inner core shear waves, *Geophys. J. Int.,* **142,** 67–73.

Deuss, A., Irving, J. & Woodhouse, J., 2010. Regional variation of inner core anisotropy from seismic normal mode observations, *Science,* **328,** 1018–1020.

Fearn, D., Loper, D. & Roberts, P., 1981. Structure of the Earth's inner core, *Nature,* **292,** 232–233.
Iritani, R., Takeuchi, N. & Kawakatsu, H., 2010. Seismic attenuation structure of the top half of the inner core beneath the northeastern Pacific, *Geophys. Res. Lett.,* **37,** L19303, doi:10.1029/2010GL044053.
Irving, J. & Deuss, A., 2011. Hemispherical structure in inner core velocity anisotropy, *J. geophys. Res.,* **16,** 4307–4323.
Kazama, T., Kawakatsu, H. & Takeuchi, N., 2008. Depth-dependent attenuation structure of the inner core inferred from short-period Hi-net data, *Phys. Earth. planet. Inter.,* **167,** 155–160.
Kennett, B., Engdahl, E. & Buland, R., 1995. Constraints on seismic velocities in the Earth from travel times, *Geophys. J. Int.,* **122,** 108–124.
Leyton, F. & Koper, K.3, 2007. Using PKiKP coda to determine inner core structure: 2. Determination of Qc, *J. geophys. Res.,* **112,** 5317–533.
Loper, D., 1983. Structure of the inner core boundary, *Geophys. astr. Fluid.,* **25,** 139–155.
Love, A., 1927, *A Treatise on the Mathematical Theory of Elasticity,* Cambridge Univ. Press.
Mäkinen, A. & Deuss, A., 2013. Normal mode splitting function measurements of anelasticity and attenuation in the Earth's inner core, *Geophys. J. Int.,* **194**(1), 401–416.
Monnereau, M., Calvet, M., Margerin, L. & Souriau, A., 2010. Lopsided growth of Earth's inner core, *Science,* **328,** 1014–1017.
Morelli, A., Dziewoński, A. & Woodhouse, J., 1986. Anisotropy of the inner core inferred from PKIKP travel times, *Geophys. Res. Lett.,* **13,** 1545–1548.
Oreshin, S. & Vinnik, L., 2004. Heterogeneity and anisotropy of seismic attenuation in the inner core, *Geophys. Res. Lett.,* **31,** 2613–2616.
Ouzounis, A. & Creager, K., 2001. Isotropy overlying anisotropy at the top of the inner core, *Geophys. Res. Lett.,* **28,** 4331–4334.
Poupinet, G., Pillet, R. & Souriau, A., 1983. Possible heterogeneity of the Earth's core deduced from PKIKP travel times, *Nature,* **305,** 204–206.
Roberts, P., Jones, C. & Calderwood, A., 2003, Energy fluxes and Ohmic dissipation in the Earth's core, in *Earth's Core and Lower Mantle,* pp. 100–129, eds Jones, C., Soward, A. & Zhang, K., Taylor & Francis.
Romanowicz, B. & Durek, J., 2000. Seismological constraints on attenuation in the Earth: a review, *Geophys. Monogr.,* **117,** 161–180.
Shearer, P., 1994. Constraints on inner core anisotropy from PKP(DF) travel times, *J. geophys. Res.,* **99,** 19 647–19 659.
Shimuzu, H., Poirier, J. & Le Mouël, J., 2005. On crystallization at the inner core boundary, *Phys. Earth. planet. Inter.,* **151,** 37–51.
Singh, S., Taylor, M. & Montagner, J., 2000. On the presence of liquid in Earth's inner core, *Science,* **287,** 2471–2474.
Song, X. & Helmberger, D., 1998. Seismic evidence for an inner core transition zone, *Science,* **282,** 924–927.
Souriau, A., 2009. Inner core structure: constraints from frequency dependent seismic anisotropy, *C. R. Geosci.,* **341,** 439–445.
Souriau, A. & Romanowicz, B., 1996. Anisotropy in inner core attenuation: a new type of data to constrain the nature of the solid core, *Geophys. Res. Lett.,* **23,** 1–4.
Souriau, A. & Roudil, P., 1995. Attenuation in the uppermost inner core from broad-band GEOSCOPE PKP data, *Geophys. J. Int.,* **123,** 572–587.
Sumita, I. & Olsen, P., 1999. A laboratory model for convection in Earth's core driven by a thermally heterogeneous mantle, *Science,* **286,** 1547–1549.
Tanaka, S. & Hamaguchi, H., 1997. Degree one heterogeneity and hemispherical variation of anisotropy in the inner core from PKP(BC)–PKP(DF) times, *J. geophys. Res.,* **102,** 2925–2938.
Tseng, T. & Huang, B., 2001. Depth-dependent attenuation in the uppermost inner core from the Taiwan short period seismic array PKP data, *Geophys. Res. Lett.,* **28,** 459–462.
Waszek, L. & Deuss, A., 2011. Distinct layering in the hemispherical seismic velocity structure of Earth's upper inner core, *J. geophys. Res.,* **116,** 12 313–12 326.
Waszek, L., Irving, J. & Deuss, A., 2011. Reconciling the hemispherical structure of Earth's inner core with its super-rotation, *Nature Geosci.,* **4,** 264–267.
Wen, L. & Niu, F., 2002. Seismic velocity and attenuation structures in the top of the Earth's inner core, *J. geophys. Res.,* **107,** 2273–2285.
Woodhouse, J., Giardini, D. & Li, X., 1986. Evidence for inner core anisotropy from free oscillations, *Geophys. Res. Lett.,* **13,** 1549–1552.
Yu, W. & Wen, L., 2006a. Seismic velocity and attenuation structures in the top 400 km of the Earth's inner core along equatorial paths, *J. geophys. Res.,* **111,** 243–253.
Yu, W. & Wen, L., 2006b. Inner core attenuation anisotropy, *Earth. planet. Sci. Lett.,* **245,** 581–594.
Yu, W. & Wen, L., 2007. Complex seismic anisotropy in the top of the Earth's inner core beneath Africa, *J. geophys. Res.,* **112,** 8304–8321.
Zou, Z., Koper, K. & Cormier, V., 2008. The structure of the base of the outer core inferred from seismic waves diffracted around the inner core, *J. geophys. Res.,* **113,** 5314–5326.

SUPPORTING INFORMATION

Additional Supporting Information may be found in the online version of this article:

Figure S1. Frequency histogram showing the distribution of signal-to-noise ratios for PKIKP.
Table S1. Results of *t*-test and *f*-tests examining the significance in the hemispherical structures.
Table S2. Results of regression of amplitude ratios, to investigate the significance of coefficients of anisotropy (eq. 3).
(http://mnras.oxfordjournals.org/lookup/suppl/doi:10.1093/gjiras/ggt368/-/DC1).

Please note: Oxford University Press is not responsible for the content or functionality of any supporting materials supplied by the authors. Any queries (other than missing material) should be directed to the corresponding author for the article.